

# Deblurring from highly incomplete measurements for remote sensing

JIANWEI MA <sup>1</sup>, FRANCOIS-XAVIER LE DIMET <sup>2</sup>

<sup>1</sup> School of Aerospace, Tsinghua University, Beijing 100084, China

E-mail: jma@tsinghua.edu.cn

<sup>2</sup> Lab. Jean-Kuntzman, University of Grenoble, BP 53, 38041 Grenoble Cedex 9, France

E-mail: Francois-Xavier.Le-Dimet@imag.fr

## Abstract

When we take photos, we often get blurring pictures because of hand shake, motion, insufficient light, unsuited focal length, or other disturbances. Recently, a compressed-sensing (CS) theorem which provides a new sampling theory for data acquisition has been applied for medical and astronomic imaging. The CS make possible to take super-resolution photos only using one or a few pixels rather than million pixels by conventional digital camera. Here we further consider a so-called compressed-sensing deblurring problem: can we still obtain clear pictures from highly incomplete measurements when blurring disturbances occur? A decoding algorithm based on Poisson singular integral and iterative curvelet thresholding is proposed to recover the deblurring problem with surprisingly incomplete measurements. It permits to design robust and practical compressed-imaging instruments involving less imaging time, less storage space, less power consumption, smaller size and cheaper than current-used CCD (charged coupled device) cameras, which match effective needs especially for probes sent very far away. It essentially shifts the on-board imaging cost to off-line recovery computational cost. Potential applications in aerospace remote sensing of Chinese Chang'e-1 lunar probe are presented.

## Index Terms

Compressed sensing/compressive sampling, single-pixel camera, deconvolution, curvelets,

sparse recovery, aerospace remote sensing.

## I. INTRODUCTION

Remote sensing by satellites and aerospace probes is an important approach for deep-space exploration. Chang'e-1 lunar probe, China's first circumlunar satellite, blasted off on a Long March 3A carrier rocket on October 24, 2007. The landmark satellite launch marked the first step of China's three-stage moon mission, which will lead to a moon landing and launch of a moon rover around 2012. One of scientific objectives of Chang'e-1 is to capture three-dimensional survey of the moon's surface and digital pictures of the Earth by remote sensing. This involves two steps: imaging by a stereo CCD camera and transmit the data back to earth.

Based on conventional imaging's principle, several million of pixels have to be stored momentarily when we take a picture using a megapixel camera. More pixels are often needed for a higher resolution. They require a huge storage space in memory or hard disk. In order to reduce the storage, an immediate data compression takes place inside the camera by an embedded tiny microprocessor performing a discrete cosine transform for JPEG format or a discrete wavelet transform for JPEG 2000 format. Discarding lots of small coefficients of the transform of the image and then reconstructing the compressed picture in retaining significant coefficient, in fact only a limited numbers of coefficients are saved for later processing. The procedure is extremely wasteful for massive data acquisitions, especially for large-scale aerospace remote sensing and require much energy from batteries. On the other hand, in order to transmit the data collected by satellites back to earth, we have to achieve huge compression ratios and consequently introducing inevitable distortions and mosaic artifacts. The question is can we record one or several pixels to improve the problems of storage, power consumption and transmission, without degrading the spatial resolution and the quality of

pictures?

In [39], we have applied a compressed-imaging technique, named CS camera, to remote sensing, which could be the next generation of imaging systems for satellites including Chinese lunar probes. Two prototypes of CS camera including single-pixel but multi-time (SPMT) cameras [1, 26] and multi-pixel but single-time (MPST) cameras have been studied. This new-generation camera is inspired by a seminal CS theorem proposed by Candès, T. Tao and J. Romberg [8–11], and Donoho [22]. The CS theorem says that compressible signals/scenes can be reconstructed from fewer measurements than traditional methods used. The traditional methods are limited by the Shannon/Nyquist sampling theorem: the sampling rate must be at least twice the maximum frequency of signals, while the CS method does not need to obey the Shannon theorem. The compressibility means that the signals are spatially sparse or with sparse transform, i.e., most of the coefficients of the signals are null in a transform domain and therefore the signals can be represented by a few coefficients. Actually, most natural scenes are compressible in suitable transforms such as Fourier, wavelets and curvelets [15, 37]. A few extensions and potential applications of CS theorem have been made [1, 7, 12, 26, 32, 35, 45, 48] in compressive imaging, wireless sensing, analogical-digital conversion, biosensing for DNA microarrays, optical architecture, astronomy, and seismic exploration. The advantages of compressed sensing are numerous, but one should keep in mind that, in most cases, compressed sensing avoids further compression of the data with classical approaches because it directly captures the compressed/geometric information in the sensing step, and ultimately that the final compression rate is usually lower than the one achieved with a classical sensor and an ad-hoc compression strategy. Remote sensing can benefit from the CS theorem in following aspects [7, 39].

- 1) One can use a single sensor (e.g., SPMT camera) or a few sensors (e.g., MPST camera)

for imaging and therefore reducing the size of cameras, thus the weight of satellites.

2) The imaging time and power consumption can be reduced due to without use of the compression step.

3) Less data are required to recover the super-resolution photos and consequently the storage space is dramatically reduced.

4) The highly compressed data taken by CS cameras can be easily transmitted back to earth.

5) Single-pixel cameras can work well for low light and outside the visible spectrum : a useful property for night-vision and infrared imaging [26].

In this paper, following [39], we will consider a more general compressed imaging: how can we obtain high-resolution pictures, using a small set of incomplete measurements, when unsuitable focal length or disturbance occurs? The technique defined hereinafter will be named compressed-sensing deblurring.

In the remainder of this paper, in section II, we first present, from the mathematical viewpoint, the problem of compressed sensing deblurring. Then, in section III, we give an outline of encoding. In section IV, we consider the decoding step by taking advantage of Poisson singular integral (PSI) deblurring operator and iterative wavelet/curvelet thresholding. Numerical experiments on standard image data and remote sensing data are shown in section V. Finally, we draw conclusions and give indications on future works in section VI.

## II. COMPRESSED-SENSING DEBLURRING

Deblurring is a inverse problem encountered in a wide variety of signal and image processing fields including physical, optical, medical, and astronomical applications. For instance, practical observed images by satellite or telescopes are usually blurred due to effects of the limitations of aperture, focal length, motion, or atmospheric turbulence. The problem of

deblurring can be symbolically stated as:

$$y = Hf + \epsilon. \quad (1)$$

Here  $f$  is an unknown original discrete signal of size  $N \times 1$ ,  $H$  is a  $N \times N$  lowpass linear blurring operator,  $\epsilon$  is measurement error or noise, and  $y$  is the observed signal. The goal of deblurring is to retrieve  $f$  from  $y$ ,

$$\tilde{f} = H^{-1}y = f + H^{-1}\epsilon. \quad (2)$$

The nonlinear deblurring processing is a mathematically ill-posed problem, which can be interpreted as the inversion of a lowpass filtering, a backward-forward diffusion, or a minimization of entropy. One serious problems is the amplification of noise by  $H^{-1}$ . The basic idea is to find a new inverse operator  $P^{-1}$

$$\tilde{f} = P^{-1}y = P^{-1}Hf + P^{-1}\epsilon, \quad (3)$$

such that  $P^{-1}Hf \approx f$  and  $P^{-1}\epsilon \approx 0$ . For instance, in [16, 36], a choice of  $P^{-1}$ , based on Poisson singular integral (PSI), is proposed to recover detailed textural components.

In this paper, we consider the deblurring problem with incomplete measurements, we have:

$$y = \Phi Hf + \epsilon. \quad (4)$$

Where  $\Phi \in \mathbb{C}^{K,N}$ ,  $K \ll N$  is a so-called CS measurement matrix or a lens-based optical imaging architecture. The recovery of the  $N \times 1$  signal  $f$  from the observation  $y$  of dimension  $K \times 1$  leads to an underdetermined system, which is an ill-posed problem. But CS theorem told us that a signal  $f$  can be exactly or accurately reconstructed from a small set of incomplete measurements, if the signal is compressible by a sparsity transform  $\Psi$  and if

the measurement matrix is incoherent/uncorrelated to this sparsity transform. [8, 9, 12, 22].

In this case, we have:

$$y = \Phi H \Psi \vartheta + \epsilon, \quad \vartheta = \Psi^{-1} f \quad (5)$$

where the  $\Psi^{-1}$  is a forward sparse transform and  $\Psi$  is its inverse.

Regularization methods are often employed for ill-posed problems to obtain a solution satisfying some criteria. Generally, the regularization can be formulated as a minimization problem with sparsity constraints:

$$\min_f \|y - \Phi H f\|_{l_2} + \lambda \|\Psi^{-1} f\|_{l_p}. \quad (6)$$

Or the recovery of the sparse coefficients  $\vartheta$  can be carried out by  $l_1$ -minimization,

$$\min_{\vartheta} \|y - \Phi H \Psi \vartheta\|_{l_2} + \lambda \|\vartheta\|_{l_1}. \quad (7)$$

The first term is a penalty term evaluating the discrepancy between the solution and the observation. The second term is a regularization term that represents the a-priori information of original scene. The  $\Psi^{-1}$  can be interpreted a regularization operator, and  $\lambda$  is a regularization parameter that can be tuned. Many regularization methods have been devised by designing different  $\Psi^{-1}$  with regard to different a-priori knowledge, such as Tikhonov regularization, total variation (TV) regularization, wavelet and Bayesian regularization, see e.g. [4, 23, 33, 42, 44]. A main problem for most existing deblurring methods is that they fail to recover textural components. Of course, the previous methods were not designed for the CS deblurring problem. In this paper, we apply a curvelet regularization and PSI deblurring operator in CS deblurring to recover textures and detailed features. The a-priori knowledge that we will use is that the scene is compressible by curvelet transform, and that a wide class of nonsmooth images can be accommodated by  $\Lambda(\alpha, p, q)$  in PSI (see detailed description of PSI in section IV).

To make the CS work well, one must successfully handle two items: encoding and decoding. The issue of encoding is to build good measurement matrices for compressed images. In fields of remote sensing and other imaging applications, the measurement matrix is actually an optical imaging system. So we also interpret the CS camera as an optical computer. Decoding means to design a nonlinear recovery algorithm for the deblurring problems with highly incomplete sensing. In aerospace remote sensing, the encoding is implemented by the on-board optical computer in satellite or probe, and decoding is carried out by ground digital computers that undertake most of the computational complexity. The CS makes us rethink the sensing mechanism. It essentially shifts the imaging cost to off-line computational cost, which is very significant to reduce the imaging time, storage space, power consumption of the on-board battery.

### III. ENCODING: COMPRESSED IMAGING

To construct the CS matrices, Candès et al. [8,11] proposed a sufficient condition, named restricted isometry property (RIP). A measurement matrix  $\Phi$  satisfies the RIP of order  $S$  with a constant  $\delta_S \in (0, 1)$ , if

$$(1 - \delta_S)\|x\|_{l_2}^2 \leq \|\Phi_T x\|_{l_2}^2 \leq (1 + \delta_S)\|x\|_{l_2}^2, \quad x \in R^N, |T| \leq S. \quad (8)$$

Here the  $\Phi_T$ ,  $T \subset 1, \dots, N$  denotes the  $K \times |T|$  submatrix obtained by extracting the columns of  $\Phi$  corresponding to the indices in  $T$ , where  $T$  is an index set of columns from measurement matrix  $\Phi$ . The RIP says that the mapping  $\Phi$  acts like an isometry on  $S - sparse$  vectors ( $S - sparse$  means the signal only has  $S$  nonzero coefficients in a transform domain). It requires that every set of columns with cardinality less than  $S$  approximately behaves like an orthonormal system. That is to say all subsets of  $S$  columns taken from  $\Phi$  are nearly orthogonal (it can not be exactly orthogonal since we have more columns than rows).

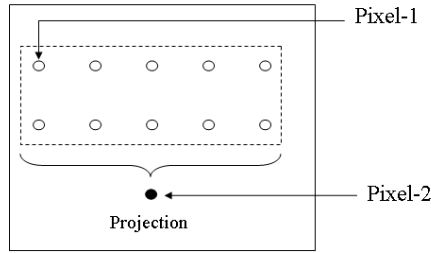


Fig. 1. Schematic comparison of the use of pixels between conventional digital cameras (as shown by Pixel-1) and CS cameras (as shown by Pixel-2). Pixel-2 is actually a compressed projection of original pixels by measurement matrices.

The measurement  $\Phi$  satisfying the RIP ensures that an exact and unique recovery will be obtained. The RIP can also be represented in the domain of the coefficients :

$$(1 - \delta_S)\|\vartheta\|_{l_2}^2 \leq \|(\Phi\Psi)_T\vartheta\|_{l_2}^2 \leq (1 + \delta_S)\|\vartheta\|_{l_2}^2, \quad \vartheta \in R^N, \|T\| \leq S \quad (9)$$

where  $\Phi\Psi$  is the measurement matrix satisfying RIP.

Roughly speaking, the measurement matrix should evaluate, in priority, the global and medium level information instead local information at the pixel level. The measurement matrix  $\Phi$  should be noise-like incoherent/uncorrelated in the sparse transform domain, i.e., there is almost no correlation between the columns of matrix  $\Phi\Psi$ . The greater incoherence is, the smaller number of measurements is needed. Frequent-used measurements are random matrices because they are incoherent to most sparse transforms. So far, a few special CS measurement matrices have been presented in order to reduce the number of measurements, including sparse 0/1 random matrices [2], Toeplitz block matrices [51], structurally random matrices and scrambled block Hadamard ensemble [30], etc. The optimal design of the measurement matrices has been studied by Elad [25]. Moreover, building determined measurement matrices satisfying a modified RIP was considered by DeVore [20].

CS-based cameras directly sense geometric and structural information by measuring compressed transform coefficients, rather than recording pixels of the scene under view as

conventional digital cameras. As shown in Figure 1, the pixel in compressed sensing actually is a projection of multipixel information by measurement matrices. Based on the CS theorem, a prototype of single-pixel CS camera has been proposed by Baraniuk et al. [1, 26] of Rice University. It collects the incoherent measurements using a digital micromirror array, and requires just one photosensitive sensor instead of millions. A single pixel here is worth a thousand words and is plenty for a picture, as Baraniuk said. This means the compression step has been cut because compression is made by imaging itself, permitting to reduce data acquisition, power and storage space. Moreover, fewer light detectors are needed in CS cameras thus saving the cost of expensive detectors. The single-pixel camera is basically an optical computer comprising two lenses, a single photon detector, an analogical-digital converter and a digital micromirror device (DMD). To provide a mathematical interpretation, first the 2D image is transformed/reshaped into a 1D signal  $x = \{x_1, \dots, x_i, \dots, x_N\}$ , then the 2D  $\Phi$  matrix is assembled using 0/1 random vector  $\Phi_m = \{\Phi_{m,1}, \dots, \Phi_{m,i}, \dots, \Phi_{m,N}\}$ , ( $m = 1, \dots, K$ ) in each row. The random vector  $\Phi_m$  is steered by orienting a bacterium-sized mirrors in DMD. The reflecting light field is focused, by lens, on the single photodiode, in order to get one measurement  $y_m = \sum_{i=1}^N \Phi_{m,i} x_i$ . Repeating  $K$  times this operation using different  $\Phi_m$  we obtain all measurements  $y = \Phi x$ . The camera is single-pixel but multi-times (SPMT) imaging. It uses a single pixel sensor which integrates during the time the result of a random sampling of the focal plane of the sensor. It can also work much with low light and outside the visible spectrum and therefore it can be used for night-vision and infrared imaging.

We can consider other measurement matrices, e.g., random undersampling of Fourier transform,  $\Phi = R \cdot F$  [35, 38]. The Fourier measurements are broadly used for x-ray imaging in medical engineering and astronomy. In this case,  $x$  is a 2-D function in the CS recovery algorithm and we obtain the  $K$  measurements at the same time by using random mask  $R$

for Fourier coefficients of  $x$ . This camera is multi-pixel but single-time (MPST) imaging. In this case, one needs lots of sensors instead of single sensor as in SPMT. Nevertheless, the number of total sensors is still much smaller than in classical cameras. Generally, one needs a ratio measurements/sensors around 0.25 to recover the original objects. By comparing the SPMT and MPST, we can say that CS cameras take a trade-off between the space and time. If we use single pixel to save space then we have to take temporal measurements to complete the imaging procedure. The image will not undergo the time delay because millions of measurements can be carried out in a fraction of second. For both CS cameras, high-resolution pictures can be recovered accurately and stably from the incomplete measurements by solving a convex optimization problem with sparse constraints [7, 12, 28, 35, 38, 52]. Alternatively, some other prototypes for measurement matrix of CS camera have been proposed [29, 45, 47]. In the numerical experiments of this paper, the 0/1 random measurement matrix and random sampling of Fourier transform are used respectively for SPMT and MPST.

#### IV. DECODING: DEBLURRING OR RECOVERY

A few recovery algorithms for compressed sensing have been recently proposed. They are based on, e.g., linear programming [8], reweighted linear programming [13], gradient projection sparse reconstruction [28], orthogonal matching pursuit (OMP) [52], stagewise OMP [24], Bregman iteration [53], and iterative thresholding [5, 7, 18, 38, 46]. They mainly fall into three categories: Greedy pursuits, convex relaxation and combinatorial algorithms [43]. Here we follow the combinatorial iterative thresholding method for the CS deblurring problem. A Poisson singular integral (PSI) deblurring operator described below is embedded into the iterative thresholding to recover edges and textures. The motivation, to use the iterative thresholding method in this paper, is that rich sparse transforms (e.g, wavelets and curvelets) can be applied easily in the iterative framework. Also, the iterative thresholding

methods are universal and useful for general signals and can be easily incorporated, by engineers, into existing methods.

#### A. Poisson-singular-integral deblurring

Due to the lowpass nature of  $H$ , the noise is amplified in deblurring (see Eq. (2)). Deblurring algorithm can be also interpreted as estimating  $f$  from the noisy signal  $\tilde{f}$ . Over the past years, the TV regularization has become of increasing interest because of its ability to reconstruct sharp discontinuities or edges in piecewise-smooth functions. The central idea of the TV technique is to restrict the space of solution in a space  $BV(\mathbb{R}^2)$  of functions of bounded variation, equipped with the seminorm  $\int_{\mathbb{R}^2} |\nabla f| d\Omega$ . However, most natural images are not with bounded variation, see e.g. [31]. They exhibit numerous edges, singularities, localized sharp features, and various other kinds of fine-scale textures, so that their TV blows up to infinity with increasing resolution. For such cases, the TV deblurring often eliminates vital small-scale information such that textures. Wavelet-based deblurring [33,44] can improve this problem to some extent, but new artifacts arise due to the shift/rotation variance of wavelet transform. Moreover, both TV and wavelet-based methods cannot be solved explicitly under the form of analytic solutions, an iterative algorithm is required leading to an expensive computational cost and thus limiting real-time applications.

Recently, a PSI regularization has been proposed for deblurring [16,36]. The deblurring problem is reconsidered in a Lipschitz space  $\Lambda(\alpha, p, q)$ , wherein a wide class of nonsmooth images can be accommodated. It can recover textures in cases where TV deblurring completely fails. Furthermore it can be solved explicitly into Fourier space without iteration. It can be written as an explicitly deblurring operator named  $P^{-1}(x)$  directly acting on the inverse problem as described in (3). In the following we will incorporate the PSI operator into the framework of the compressed-sensing deblurring. We briefly describe the PSI regularization

in reminder of this section. For more details, we refer to [16, 36].

For a fixed  $t > 0$ , let us consider the Poisson kernel in  $R^2$

$$\varphi(x, y, t) = \frac{t}{2\pi(x^2 + y^2 + t^2)^{3/2}}, \quad (x, y) \in \mathbb{R}^2. \quad (10)$$

Define the Poisson integral operator  $U^t$  on  $L^p(R^2)$ ,  $1 \leq p < \infty$ , by

$$U^t f = \int_{\mathbb{R}^2} \varphi(\zeta, \varsigma, t) f(x - \zeta, y - \varsigma) d\zeta d\varsigma. \quad (11)$$

Define a linear operator  $Z(t)$  in  $L^2(\mathbb{R}^2)$  by [16]

$$Z(t)f = \int_{\mathbb{R}^2} \hat{z}(\xi, \eta, t) \hat{f}(\xi, \eta) e^{2\pi i(\xi x + \eta y)} d\xi d\eta, \quad \rho = \sqrt{\xi^2 + \eta^2}. \quad (12)$$

Here  $\hat{z}(\xi, \eta, t) = (t + \frac{4e^{-t\rho} - e^{-2t\rho} - 3}{2\rho})^{1/2}$ .

For any  $f \in \Lambda(\alpha, 2, \infty)$ ,  $0 < \alpha < 1$ , we have  $\|U^s f - f\|_2 \leq C_{\bar{t}} \|f\|_2 s^\alpha$ ,  $0 \leq s \leq \bar{t}$ , where  $C_{\bar{t}}$  is a positive constant. The Lipschitz space  $\Lambda(\alpha, \beta, \infty)$  considers functions  $f$  satisfying a weaker condition :

$$\left\{ \int_{\mathbb{R}^2} |f(x+h) - f(x)|^\beta dx \right\}^{1/\beta} \leq Const |h|^\alpha, \quad (13)$$

than the BV space for which  $\alpha = 1$  and  $\beta = 1$ . For most natural scenes, we have  $0.2 < \alpha < 0.7$ . Functions with larger values of  $\alpha$  are smoother than those with smaller values of  $\alpha$ .

For a function  $f$  the deblurring PSI-regularized  $f^\varphi$  can be defined by :

$$f^\varphi(x, y) = \arg \min_{f \in L^2(\mathbb{R}^2)} \{ \|Hf - y\|_2^2 + (\epsilon/M)^2 (\|f\|_2^2 + \Gamma_{\bar{t}}^2 \|Z(\bar{t})f\|_2^2) \}, \quad (14)$$

where the parameters  $\epsilon$ ,  $M$ , and  $\Gamma_{\bar{t}}$  satisfy

$$\|Hf - y\|_2 \leq \epsilon, \quad \|f\|_2 \leq M, \quad \Gamma_{\bar{t}} = \left\{ \frac{1 + 2\alpha}{C_{\bar{t}}^2 \bar{t}^{1+2\alpha}} \right\}^{1/2}. \quad (15)$$

$f^\varphi$  can be found explicitly in Fourier space by

$$\hat{f}^\varphi(\xi, \eta) = \frac{\tilde{H}(\xi, \eta) \hat{y}(\xi, \eta)}{|\hat{H}(\xi, \eta)|^2 + (\epsilon/M)^2 \{1 + \Gamma_{\bar{t}}^2 |\hat{z}(\xi, \eta, \bar{t})|^2\}}. \quad (16)$$

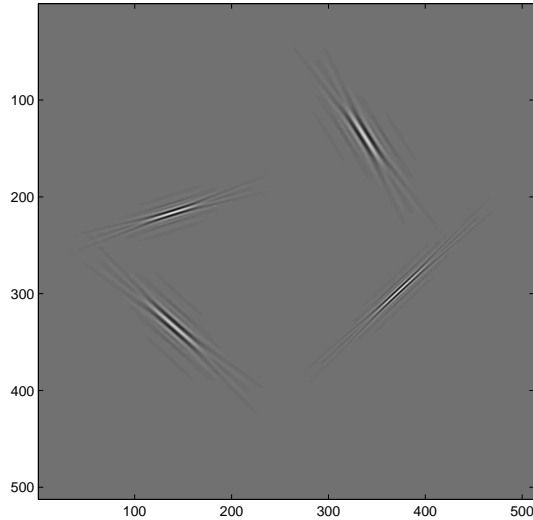


Fig. 2. Elements of curvelets in spatial domain.

For  $\Gamma_{\bar{t}} = 0$ , the method correspond to the classical Tikhonov deblurring. The main parameter is  $\alpha$ , which is related to the smoothness of recovered images. Smaller values of  $\alpha$  lead to recovered images with more detailed features.

We define the PSI deblurring operator  $P^{-1}$  by the inverse Fourier transform of  $\hat{f}^\varphi$ .

### B. Nonlinear recovery by iterative curvelet thresholding

Curvelet transform [14,15] is a new geometric multiscale transform. As wavelet transform owns good performance to represent isotropic point singularities, curvelet transform allows an optimal sparse representation of objects with  $C^2$  singularities. The needle-shape elements of this transform own very high directional sensitivity and anisotropy (see Fig. 2). For a smooth object  $f$  with discontinuities along smooth curves, the best  $m$ -term approximation  $\tilde{f}_m$  by curvelet thresholding obeys  $\|f - \tilde{f}_m\|_2^2 \leq Cm^{-2}(\log m)^3$ , while for wavelets the decay rate is only  $m^{-1}$ .

Unlike wavelets, indexed by two parameters, a system of curvelets is indexed by three parameters. Let  $\mu$  be the collection of triple index  $(j, l, k)$ , where  $j, l$  and  $k = (k_1, k_2)$  are respectively scale, orientation and translation parameters. The curvelets are defined as

functions of  $x \in \mathbb{R}^2$  by

$$\psi_\mu(x) = \psi_j(R_{\theta_J}(x - k_\delta)). \quad (17)$$

In the above,  $\psi$  is a waveform oscillatory in the horizontal direction and bell-shaped (nonoscillatory) along the vertical direction.  $R_{\theta_J}$  is a rotation matrix of angle  $\theta_J = 2\pi \cdot 2^{-\lfloor j/2 \rfloor} \cdot l$ ,  $J = (j, l)$  indexing the scale/angle, with  $\lfloor \cdot \rfloor$  denoting the integer part, while the translation parameter is given by  $k_\delta = R_{\theta_J}^{-1}(k_1 \cdot 2^{-j}, k_2 \cdot 2^{-j/2})$ . The curvelet elements are obtained by anisotropic dilations, rotations and translations of a collection of unit scale oscillatory blobs. For a function  $f$  the curvelet coefficients are given by :

$$c_\mu = \langle f, \psi_\mu \rangle = \int_{\mathbb{R}^2} f(x) \bar{\psi}_\mu(x) dx, \quad (18)$$

and it can be directly evaluated in the frequency domain. Introduce the 2D frequency window

$$W_j(\omega) = 2^{-3j/4} w(2^{-j} |\omega|) v\left(\frac{2^{\lfloor j/2 \rfloor} \theta}{2\pi}\right), \quad (19)$$

where the radial window  $w$  (e.g., Meyer wavelet window) partitions the frequency domain into annuli  $|x| \in [2^j, 2^{j+1})$  and the angular window  $v$  partitions the annuli into wedges  $\theta_J$ . By defining the curvelets in the frequency domain  $\hat{\psi}_\mu(\omega) = W_j(R_{\theta_J}\omega) e^{-i\langle k_\delta, \omega \rangle}$ , i.e. taking oriented local Fourier bases on each wedge, and using Plancherel theorem for Eq. (18), we get :

$$c_\mu = \frac{1}{(2\pi)^2} \int \hat{f}(\omega) \bar{\hat{\psi}}_\mu(\omega) d\omega = \frac{1}{(2\pi)^2} \int \hat{f}(\omega) W_j(R_{\theta_J}\omega) e^{i\langle k_\delta, \omega \rangle} d\omega. \quad (20)$$

The forward and inverse curvelet transform have the computational cost of  $\mathcal{O}(N^2 \log N)$  for an  $(N \times N)$  image. We refer to [14, 15, 37, 41, 50] for more details on curvelets and their applications.

Let us define the following thresholding function :

$$S_\tau(f, \Psi) = \sum_\mu \tau(c_\mu(f)) \psi_\mu, \quad (21)$$

where  $\tau$  can be taken as a soft thresholding function defined for a fixed threshold  $\sigma > 0$ ,

$$\tau_s(x) = \begin{cases} x - \sigma, & x \geq \sigma, \\ 0, & |x| < \sigma, \\ x + \sigma & x \leq -\sigma, \end{cases}$$

or a hard thresholding function

$$\tau_h(x) = \begin{cases} x, & |x| \geq \sigma, \\ 0, & |x| < \sigma, \end{cases}$$

or the continuous garrote thresholding

$$\tau_g(x) := \begin{cases} x - \frac{\sigma^2}{x}, & |x| \geq \sigma, \\ 0, & |x| < \sigma, \end{cases}$$

which may be a good choice and such that large coefficients nearly remain unaltered. In practice the choice of a thresholding function and threshold value  $\sigma$  depends on the objects that we want to discern. The choice of an optimal  $\sigma$  for a specific applications is an open problem. In this paper, we use the simplest hard thresholding function with a decreasing threshold values after each iteration.

By minimizing a surrogate functional [18], we can obtain the solution by iterating thresholding function

$$S_\tau(f + P^{-1}\Phi^T(y - \Phi H f), \Psi). \quad (22)$$

Here we use the PSI deblurring operator  $P^{-1}$  instead of the inverse operator  $H^{-1}$ .

The algorithm can be summarized as :

1) Initialization: set the iteration index  $p = 0$ , initial value  $f_0 = 0$  or a reconstruction by zero-filling with density compensation (zf-w/dc) of initial incomplete measurements [35].

2) Updating the estimation:

$$\tilde{f}_p = f_p + P^{-1}\Phi^T(y - \Phi H f_p).$$

3) Thresholding for curvelet transform of the updated estimation:

$$f_{p+1} = S_\tau(\tilde{f}_p, \Psi).$$

4) Iteration: If  $\|f_{p+1} - f_p\| > \varepsilon$ , then set  $p+1$  to  $p$  and go to step 2, else stop iterations.

5) Alternatively, in the last iterations, or after ending iterations, one can apply TV-synthesis curvelet thresholding [40], which can suppress the pseudo-Gibbs artifacts (small high-frequency oscillations due to a false reconstruction of the fine-scale coefficient components) and element-like artifacts while preserving the discontinuities associated to edges and other features. Here the TV of a function  $f$  with  $|\nabla f \in L^1(\Omega)|$  is defined by  $TV(f) = \int_\Omega |\nabla u(\zeta)| d\zeta$  [49]. Thresholding is defined as an optimization problem involving the total variation norm and a constraint on the curvelet space. It can be interpreted as a projected iterative thresholding. Essentially, TV minimization keeps the significant coefficients unchanged, and meanwhile does not set the insignificant coefficients to zero as conventional shrinkage does, but gives to these coefficients optimal small values in order to eliminate the artifacts.

In terms of the decoding, the MPST camera is faster than SPMT camera because the CS measurement matrix  $\Phi$  in MPST has much smaller size than those used in SPMT. For instance, assuming  $K$  measurements for a  $(N \times N)$  object, we have a measurement matrix  $\Phi$  with size  $K \times N$  in MPST, while one with size  $K \times N^2$  in SPMT because it sets every random measurement as a row of measurement matrix. Mathematically, the computational complexity of MPST is  $\mathcal{O}(P(4N \log N + 2N^2 \log N))$  for a  $N \times N$  object, while those of SPMT is  $\mathcal{O}(P(2KN^2 \log N + 2N^2 \log N))$  where  $\log N \leq K \leq N^2$  ( $P$  being the number of iterations).

It should be noted that some other sparse transforms, e.g. wavelets, contourlets [21], bandlets [34] and wave atoms [19], can be applied in this iterative thresholding framework.

For related mathematical convergence of the iterative thresholding framework, we refer to [18] for iterative soft thresholding, and [5, 6] for iterative hard thresholding.

## V. NUMERICAL EXPERIMENTS

We consider the deconvolution problem of image blurred by an out-of-focus model, i.e., a shift-variant point spread function (psf)  $H(x, y) = (\pi R^2)^{-1}$  when  $x^2 + y^2 \leq R^2$ , and zeros otherwise. The Fourier transform of  $H$  used in Eq. (16) can be obtained by  $\hat{H}(\xi, \eta) = 2J_1(R\rho)/(R\rho)$ , in which  $\rho = \sqrt{\xi^2 + \eta^2}$  and  $J_1$  is the one-order Bessel function.

We first show performances of the MPST CS camera. We consider 30% incomplete measurements (30% sampling points are used) and a random measurement noise produced by 0.01% random numbers. In the first case, we test a standard Lena data using our method. Fig. 3 (a) is the original Lena image. Fig. 3 (b) shows a blurred image using the above point spread function with  $R = 3$ . Furthermore, we consider a mask for Fourier coefficients of the blurred image to carry out the incomplete measurements. The Fig. 3 (c) shows the mask where the white points denote sampling points. Fig. 3 (d) shows the deblurred result using PSI operator  $P^{-1}$  and zero-filling reconstruction [35] (i.e., without iterative thresholding). While in Fig. 3 (e), we show the result reconstructed by  $H^{-1}$  defocus operator and iterative curvelet thresholding (ICT) (i.e., without the use of PSI). Fig. 3 (f) is recovered by the proposed method where the PSI is embedded into the ICT. Our method achieves much higher SNR (signal-noise-ratio). In this case, we have taken the parameters  $C_t = 0.99$ ,  $\alpha = 0.28$ ,  $t = 0.2$  for PSI, and decreasing threshold value  $\sigma_0(1 - p/L)$ , in which  $L = 40$  is the total number of iteration;  $p$  is the iteration index; the initial threshold  $\sigma_0 = 0.06$ . It can be seen that the detailed features and textures are also well recovered. If we use the additive step 5 in our algorithm, we can obtain a more clear image in terms of visual quality, but a little low SNR (45.52 dB). Fig. 4 displays the comparison of close-up of the results without

or with step 5. The right figure is the result using step 5, i.e., a TV-constrained ICT is applied in last 5 iterations. It presents less artifacts, especially in smooth area.

In Figure 5, we have applied our CS deblurring method to atmospheric remote sensing. Fig. 5 (a) is a original cloud system image mainly consisting with smooth vortex features. Fig. 5 (b) is a blurred image. All computational parameters are the same as those used in above test. Fig. 5 (c) is the deblurring result using PSI and zero-filling reconstruction (without ICT). Fig. 5 (d) is the result by our method with 40 iteration, and (e) is its recovery error that displays as random noise. Fig. 5 (f) shows the SNR vs iteration numbers by our method.

Consider another atmospheric remote sensing data with more detailed features. Figure 6 (a) is the original cloud image and (b) is a blurred image. Fig. 6 (c) is the zero-filling reconstruction, i.e., by using the PSI operator but without iterative curvelet thresholding in our CS deblurring framework. Amplified noises can be seen obviously in this result. Fig. 6 (d) is the result recovered by our method (i.e., using both the PSI and iterative curvelet thresholding), in which detailed features have been recovered well from the 30% incomplete measurements. We also study the performances of our method (in terms of SNR and error of recovered images) as function of the measurement numbers from 10% measurements to 55% measurements, as shown in Figure 7. It can be seen that 15% measurements are enough to obtain a satisfying restoration. The SNR increases as the measurement numbers increases (see Fig. 7 (a), while the recovery error (here we use  $l_1$  norm error) decreases (see Fig. 7 (b)).

Let us come back to Chang'e-1 lunar probe. In addition to the stereo design currently used CCD camera, Chang'e-1 also includes a wide-angle lens and  $1024 \times 1024$  array sensors. Fig. 8 (a) shows the first moon's picture captured by the Chang'e-1 at altitude of  $200km$

and with a resolution of  $120m$ . We have used the same blurred function and undersampling strategy (considering 30% measurements) as above test. Fig. 8 (b) shows the reconstruction using  $H^{-1}$  and zero-filling. Fig. 8 (c) is the decoding result by our method. The decreasing threshold value  $\sigma_0(1 - p/L)$  is used, with the total number of iteration  $L = 30$  and the initial threshold  $\sigma_0 = 0.06$ . Although most scenes of remote sensing consist of line-singularity features, the moon's surface displays a lot of points looking like impact craters which were produced by asteroid during the past billions of years. Based on the specific requirement on measurement of point-like features, we also test the method using wavelet thresholding in Fig. 8 (d), instead of curvelet thresholding. As we all known, the wavelets and curvelets are, respectively, optimal representation for point-like features and line/edge features. In our method, using a combining best basis strategy in our method would be promising [46].

Now let us show the performance of the SPMT camera in applications of remote sensing. In terms of the decoding, the current SPMT cameras require more memory and computational complexity than those of MPST cameras, because the matrix  $\Phi$  in SPMT has a much larger dimension those in MPST cameras. Fig. 9 (a) is part of original scenes shown in Fig. 8 (a). In this case, we use 25% incomplete measurements. Fig. 9 (b) is the recovery using single-step directly inverse, i.e.,  $x = P^{-1}\Phi^{-1}y$ . The result is totally wrong. Fig. 9 (c) is the recovery using our method. As a comparison, Fig. 9 (d) shows the result recovered when we use the  $H^{-1}$  instead of  $P^{-1}$  in our ICT. We also test the performances of our ICT method for cases with only incomplete measurement but without burring, when the number of measurement increases. Fig. 10 (a) and (b) shows the SNR and recovery error vs measurement numbers, and Fig. 10 (c) shows the computational time vs the number of measurements. One has a larger size for measurement matrices as the number of measurements increases, therefore more computational cost in the nonlinear decoding has to be paid.

With respect to the performance of the recovery procedure let us point out that, because we use the random measurement matrices instead of determinate measurement matrices, the relation of SNR vs number of measurements is not strictly increasingly monotone. The performances of the recovery procedure is mainly relate to two aspects: The first one is related to the measurement matrix (see e.g., [20, 25, 30, 51]). It must be incoherent/uncorrelated to the sparse transform. The random matrix is universal for almost cases, but it is surely not optimal for a specific case. How to construct optimal/determinate measurement matrices is a question under works by mathematicians. The second one is related to the recovery algorithm (see e.g., [3, 6, 8, 43, 52, 53]). The iterative thresholding methods depend on the sparse transforms. Using an adaptive transform by machine learning from a sparsity dictionary is a promising approach [17]. We will compare, in details, the performances of different sparse transforms involving wavelets, curvelets, adaptive bandlets and total variation method for CS remote sensing in a forthcoming paper.

By suitable design of the encoding imaging and decoding recovery algorithm, the CS imaging carries out the compression and denoising at the same time.

Although our application is focused on remote sensing, the method can be widely applied in other imaging fields.

## VI. CONCLUSIONS

CS theorem make us rethink the sensing mechanisms. It shifts the on-board imaging cost toward off-line computational cost. In this paper, we have applied two measurement strategy: single-pixel imaging and partial random Fourier measurement to deblurring of remote sensing of satellites or probes. The proposed technique impacts at least two domains of remote sensing:

- 1) Imaging by physical instrument. In the new system, the compression is implemented

by optical imaging itself. Pixel is no longer considered an ensemble of pixels. Only  $O(S \cdot \log(N/S))$  incomplete measurements are needed to recover any  $S$ -sparse  $N \times N$  pictures. Therefore, we can reduce the required pixels/sensor, and thus reduce imaging time and furthermore less storage space, less power consumption, and smaller size of cameras are possible. The CS imaging instrument is very significant when measurements are limited by physical constrains and disturbances.

2) Super-resolution imaging. The CS recovery technique can improve the resolution of pictures taken by current CCD cameras.

Another contribution of this paper is the observation that singular integral deconvolution recovers vital small-scale structures and iterative thresholding can robustly reconstruct the scenes from highly incomplete measurements. The proposed decoding method of compressed-sensing deblurring takes advantage of both of these items. High-resolution pictures can be recovered taking use of super computers on earth instead of the chip inside the on-board camera.

The presented technique opens a new and practical way for satellite remote sensing by greatly reducing the imaging time, storage space, power consumption of the on-board battery, and also reducing the number of data to be transmitted back to earth. The applications to night-vision and infrared remote sensing might be of great importance.

There is a large potential for further developments both on theoretical and practical aspects. The following suggestions might be considered as a sequel to this work:

1) Build specific CS matrices for single-pixel cameras in large-scale imaging and deblurring.

2) Design a reweighted iterative thresholding to improve the performances of decoding for remote sensing.

3) Build a practical industrial prototype of the CS camera for real-time applications in aerospace probe, and check what would be the actual gain in terms of storage/transmission/energy consumption.

4) How to apply the CS method for blind deconvolution problem when  $H$  is unknown?

5) An important motivation of this paper is to proposed a practical method for data assimilation of geophysical fluids using CS remote sensing information [41]. Applying the CS method to data assimilation for meteorological and oceanic forecast and modeling is under works.

## Acknowledgments

The first author would like to thank financial support from NSFC Grant No. 40704019, TBRF (JC2007030), PetroChina Innovation Fund (060511-1-1), and invited Professorship at Laboratoire Jean-Kuntzman of the Universite de Grenoble and INRIA-Rhne-Alpes. A partial support was provided by Agence Nationale de la Recherche (ASSIMAGE and ADDISA projects).

## REFERENCES

- [1] R. Baraniuk, A lecture on compressive sensing, *IEEE Signal Processing Magazine* **24** (4), 118-121 (2007).
- [2] R. Berinde, P. Indyk, Sparse recovery using sparse random matrices, Tech. Report of MIT, (2008).
- [3] R. Berinde, A. Geilbert, P. Indyk, H. Karloff, M. Strauss, Combining geometry and combinatorics: a unified approach to sparse signal recovery, Tech. Report of MIT, (2008).
- [4] T. Berger, J. Stromberg, T. Eltoft, Adaptive regularized constrained least squares image restoration, *IEEE Trans. Image Process.* **8** (9), 1191-1203 (1999).

- [5] T. Blumensath, M. Davies, Iterative hard thresholding for compressed sensing, Preprint, IDCAM, University of Edinburgh, (2008).
- [6] T. Blumensath, M. Davies, Iterative thresholding for sparse approximations, *J. Fourier Anal. Appl.*, to appear, (2008).
- [7] J. Bobin, J. Starck, R. Ottensmeyer, Compressed sensing in astronomy, *IEEE J. Selected Topics in Signal Process.*, submitted, (2008).
- [8] E. Candès, T. Tao, Decoding by linear programming, *IEEE Trans. Inform. Theory* **51**, 4203-4215 (2005).
- [9] E. Candès, J. Romberg, T. Tao, Stable signal recovery from incomplete and inaccurate information, *Commun. Pure Appl. Math.* **59**, 1207-1233 (2005).
- [10] E. Candès, T. Tao, Near optimal signal recovery from random projections: universal encoding strategies, *IEEE Trans. Inform. Theory* **52** (12), 5406-5425 (2006).
- [11] E. Candès, J. Romberg, T. Tao, Robust uncertainty principles: exact signal reconstruction from highly incomplete frequency information, *IEEE Trans. Inform. Theory* **52** (2), 489-590 (2006).
- [12] E. Candès, M. Wakin, An introduction to compressive sampling, *IEEE Signal Processing Magazine*, **25** (2), 21-30, (2008).
- [13] E. Candès, M. Wakin, S. Boyd, Enhancing sparsity by reweighted  $l_1$  minimization, submitted, (2007).
- [14] E. Candès, D. Donoho, New tight frames of curvelets and optimal representations of objects with piecewise singularities, *Comm. Pure Appl. Math.* **57**, 219-266 (2004).
- [15] E. Candès, L. Demanet, D. Donoho, L. Ying, Fast discrete curvelet transforms, *Multi-scale Model. Simul.* **5** (3), 8610-889 (2006).
- [16] A. Carasso, Singular integrals, image Smoothness, and the recovery of texture in image

- deblurring, *SIAM J. Appl. Math.* **64**, 1749-1774 (2004).
- [17] J. Duarete-Carvajalino, G. Sapiro, Learning to sense sparse signals: simultaneous sensing matrix and sparsity dictionary optimization, IMA Preprint 2211m, University of Minnesota, (2008).
- [18] I. Daubechies, M. De Friese, C. De Mol, An iterative thresholding algorithm for linear inverse problems with a sparsity constraint, *Commun. Pure Appl. Math.* **57**, 1413-1457 (2004).
- [19] L. Demanet, L. Ying, Wave atoms and sparsity of oscillatory patterns, *Appl. Comput. Harmon. Anal.* **23** (3), 368-387 (2007).
- [20] R. DeVore, Deterministic constructions of compressed sensing matrices, *J. of Complexity* **23**, 918 - 925 (2007).
- [21] M. Do, M. Vetterli, The contourlet transform: an efficient directional multiresolution image representation, *IEEE Trans. Image Process.* **14** (12), 2091-2106 (2005).
- [22] D. Donoho, Compressed sensing, *IEEE Trans. Inform. Theory* **52** (4), 1289-1306 (2006).
- [23] D. Donoho, Nonlinear solution of inverse problems by wavelet-vaguelette decomposition, *Appl. Comput. Harmn. Anal.* **2**, 101-126 (1995).
- [24] D. Donoho, Y. Tsaig, I. Drori, J. Starck, Sparse solution of underdetermined linear equations by stagewise Orthogonal Matching Pursuit, submitted, (2008).
- [25] M. Elad, Optimized projections for compressed sensing, *IEEE Trans. Signal Process.* **55** (12), 5695-5702 (2007).
- [26] M. Duarte, M. Davenport, D. Takhar, J. Laska, T. Sun, K. Kelly, R. Baraniuk, Single-pixel imaging via compressive sampling, *IEEE Signal Process. Mag.* **25** (2), 83-91 (2008).
- [27] M. Elad, B. Matalon, J. Shtok, M. Zibulevsky, A wide-angle view at iterated shrinkage algorithms, *Proc. of SPIE*, vol. 6701, pp. 670102:1-19, 2007.

- [28] M. Figueiredo, R. Nowak, S. Wright, Gradient projection for sparse reconstruction: application to compressed sensing and other inverse problems, *IEEE J. Select Topic in Signal Process.* **1** (4), 586-597 (2007).
- [29] R. Fergus, A. Torralba, W. Freeman, Random lens imaging, MIT CSAIL Technical Report 2006-058, 2006.
- [30] L. Gan, T. Do, T. Tran, Fast compressive imaging using scrambled block Hadamard ensemble, preprint, (2008).
- [31] Y. Gousseau, J. M. Morel, Are natural images of bounded variation? *SIAM J. Math. Anal.* **33** (3), 634-648 (2001).
- [32] G. Hennenfent, F. Herrmann. Simply denoise: wavefield reconstruction via jittered undersampling, *Geophysics*, **73** (3), 2008.
- [33] J. Kalifa, S. Mallat, B. Rouge, Deconvolution by thresholding in mirror wavelet bases, *IEEE Trans. Image Process.* **12** (4), 446-457 (2003).
- [34] E. Le Pennec, S. Mallat, Sparse geometrical image approximation with bandlets, *IEEE Trans. Image Process.* **14** (4), 423-438 (2005).
- [35] M. Lustig, D. Donoho, J. Pauly, Sparse MRI: the application of compressed sensing for rapid MR imaging, *Magnetic Resonance in Medicine* **58** (6), 1182-1195 (2007).
- [36] J. Ma, Deconvolution using singular integral regularization and curvelet shrinkage, *Phys. Lett. A* **368**, 245-250 (2007).
- [37] J. Ma, G. Plonka, Combined curvelet shrinkage and nonlinear anisotropic diffusion, *IEEE Trans. Image Process.* **16** (9), 2198-2206 (2007).
- [38] J. Ma, Compressed sensing for surface metrology, *IEEE Trans. Instrum. Measure.*, submitted, 2008.
- [39] J. Ma, Single-pixel remote sensing, *IEEE Geosci. Remote Sensing Lett.*, submitted,

2008.

- [40] J. Ma, Curvelets for surface characterization, *Appl. Phys. Lett.* **90**, 054109:1-3 (2007).
- [41] J. Ma, A. Antoniadis, F.-X. Le Dimet, Curvelet-based snake for multiscale detection and tracking of geophysical fluids, *IEEE Trans. Geosci. Remote Sensing* **44** (12), 3626-3638 (2006).
- [42] M. Mignotte, A Segmentation-based regularization term for image deconvolution, *IEEE Trans. Image Process.* **15** (7), 1973-1984 (2006).
- [43] D. Needell, J. Tropp, CoSaMP: iterative singal recovery from incomplete and inaccurate samples, *Appl. Comp. Harmonic Anal.*, to appear, (2008).
- [44] R. Neelamani, H. Choi, R. Baraniuk, ForWaRD: Fourier-wavelet regularized deconvolution for ill-conditioned systems, *IEEE Trans. Signal Process.* **52** (2), 418-433 (2004).
- [45] M. Neifeld, J. Ke, Optical architectures for compressive imaging, *Applied Optics* **46** (22), 5293-5303 (2007).
- [46] G. Peyré, Best basis compressed sensing, *Proceedings of SSVM07*, pp. 80-91, June 2007.
- [47] N. Pitsianis, et al., Compressive imaging sensors, *Proc. of SPIE*, vol. 6232, pp. 62320A:1-9, 2006.
- [48] H. Rauhut, K. Schnass, P. Vandergheynst, Compressed sensing and redundant dictionaries, *IEEE Trans. Information Theory* **54** (5), 2210-2219 (2008).
- [49] L. Rudin, S. Osher, E. Fatemi, Nonlinear total variaton noise removal algorithm, *Phys. D* **60**, 259-268 (1992).
- [50] J. Starck, E. Candès, D. Donoho, The curvelet transform for image denoising, *IEEE Trans. Image Process.* **11**, 670-684 (2002).
- [51] F. Seibert, L. Ying, Y. Zou, Toeplitz block matrices in compressed sensing, preprint, (2008).

- [52] J. Tropp, A. Gilbert, Signal recovery from random measurements via orthogonal matching pursuit, *IEEE Trans. Inform. Theory* **53** (12), 4655-4666 (2008).
- [53] W. Yin, S. Osher, D. Goldfarb, J. Darbon, Bregman iterative algorithms for  $\ell_1$  minimization with applications to compressed sensing, *SIAM J. Imaging science*, submitted, (2008).

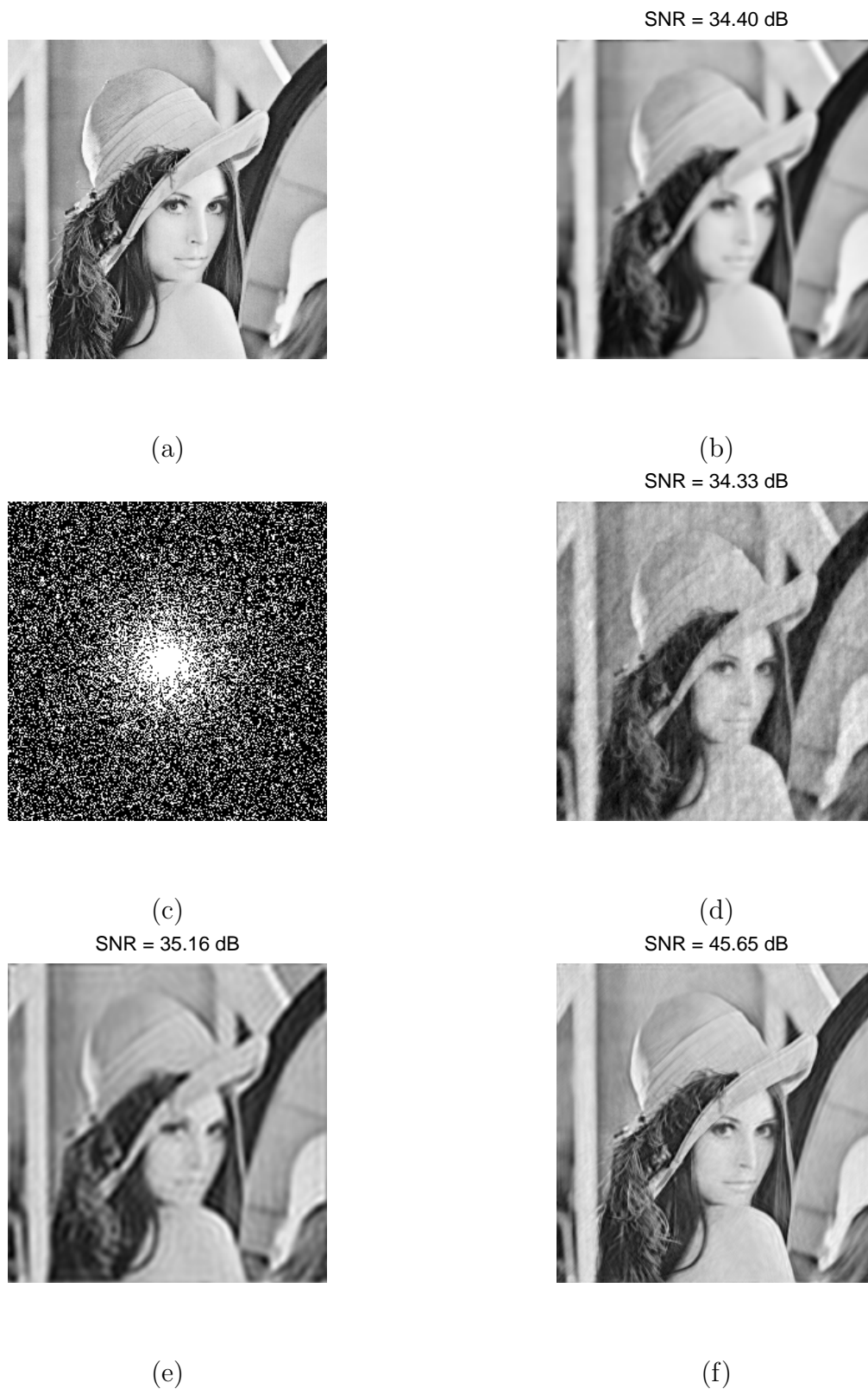
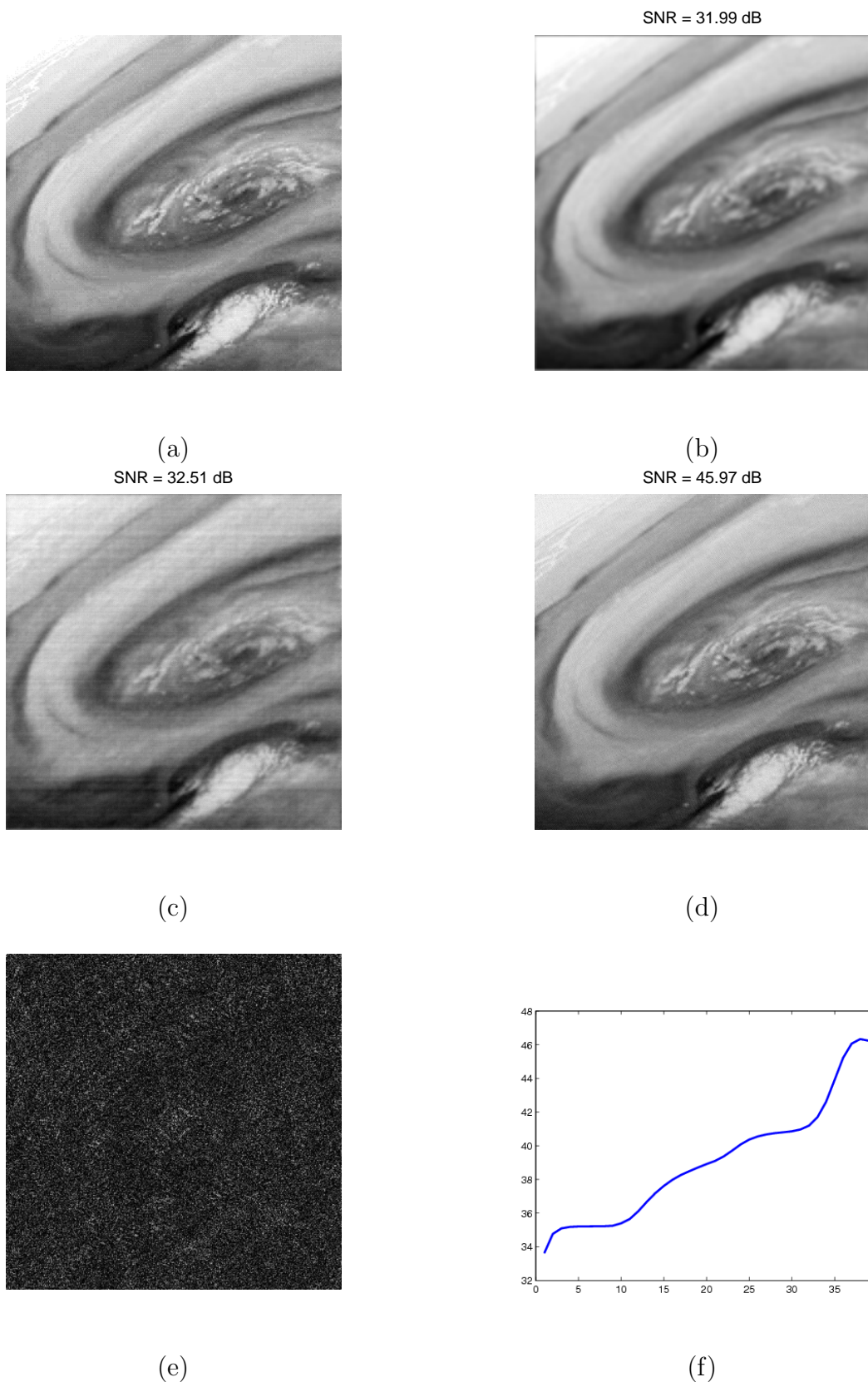


Fig. 3. CS Deblurring for a standard Lena image by MPST. (a) original image. (b) blurred image. (c) mask of incomplete measurements (white points denote the sampling points). (d) CS Deblurring using PSI and zero-filling reconstruction (without ICT). (e) using  $H^{-1}$  and ICT (without PSI). (f) using the proposed method: combination of PSI and ICT.



Fig. 4. (a) A close-up of CS Deblurring result shown in Fig. 3. (b) The result by our method with additive step 5.



July 22, 2008—11:04 am  
 Fig. 5. CS Deblurring for atmospheric remote sensing by MPST. (a) original cloud system. (b) blurred image. (c) CS Deblurring using PSI and zero-filling reconstruction (without ICT). (d) using the proposed method: combination of PSI and ICT. (e) recovery error by our method. (f) SNR vs iterative numbers by our method. DRAFT

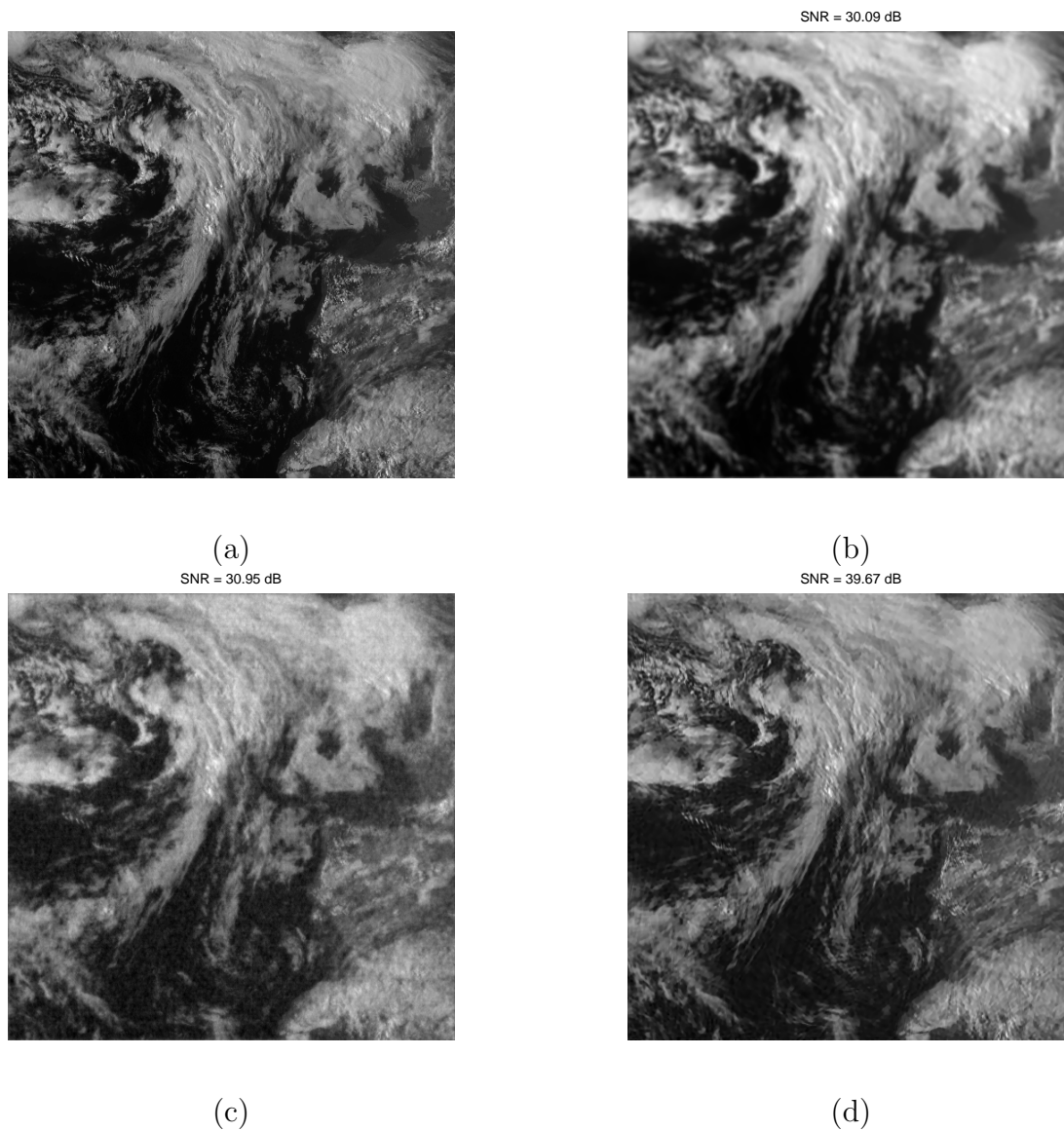
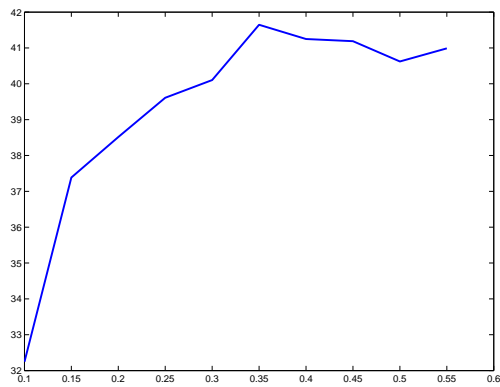
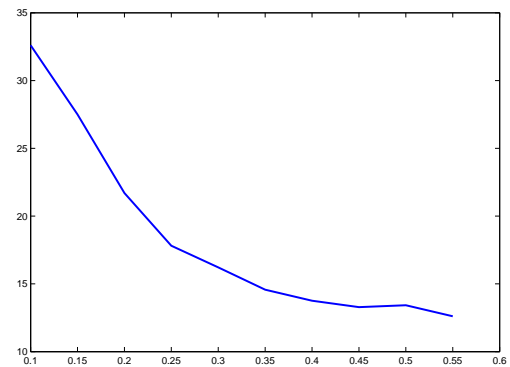


Fig. 6. CS deblurring for atmospheric remote sensing by MPST. (a) original cloud system. (b) blurred image (SNR = 30.09 dB). (c) deblurring by zero-filling reconstruction, i.e., using PSI but without ICT (SNR = 30.95 dB). (d) deblurring using our methods (using both PSI and ICT) (SNR = 39.67 dB).



(a)



(b)

Fig. 7. Performances of MPST as the number of measurements increases. (a) SNR (vertical coordinate) vs measurement numbers (horizontal coordinate). (b) Recovery error vs measurement numbers. The horizontal coordinate denotes the rate of practical measurements to total measurements.

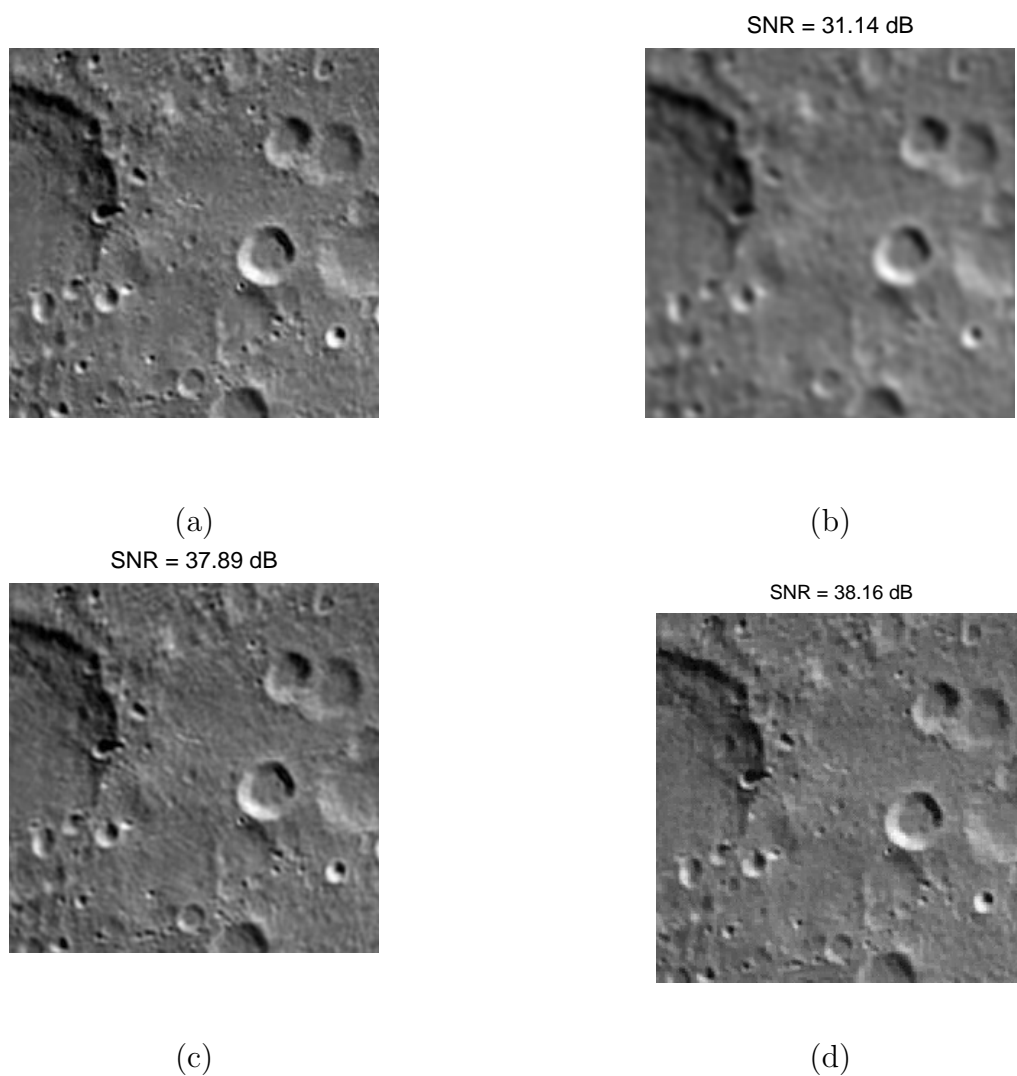


Fig. 8. CS deblurring for part of moon's surface by MPST. (a) original scene. (b) zero-filling reconstruction (SNR = 31.14 dB). (c) our method with curvelet thresholding (SNR = 37.89 dB). (d) our method with wavelets thresholding (SNR = 38.16 dB).

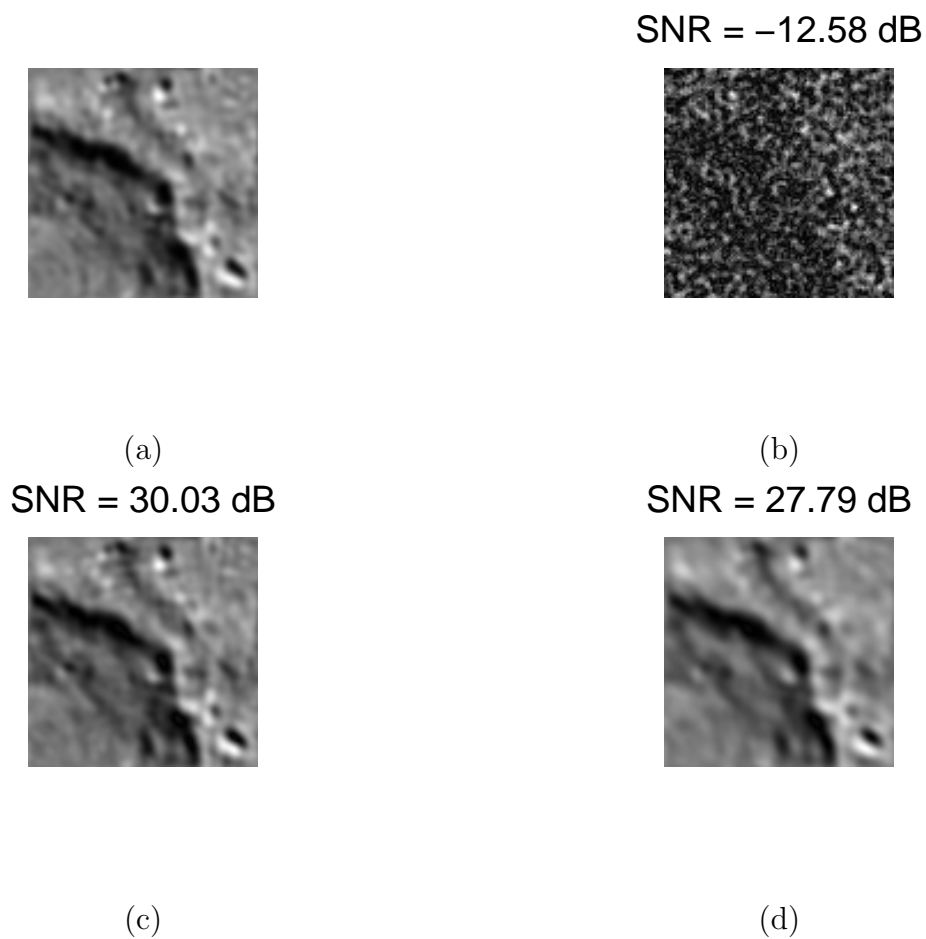
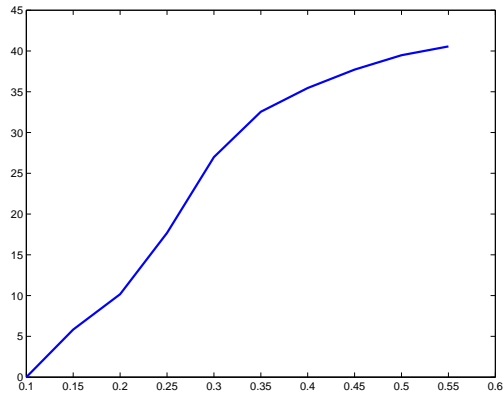
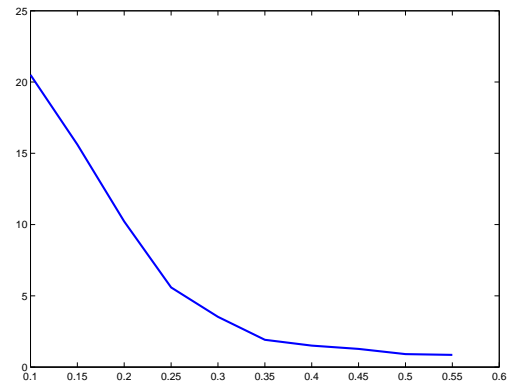


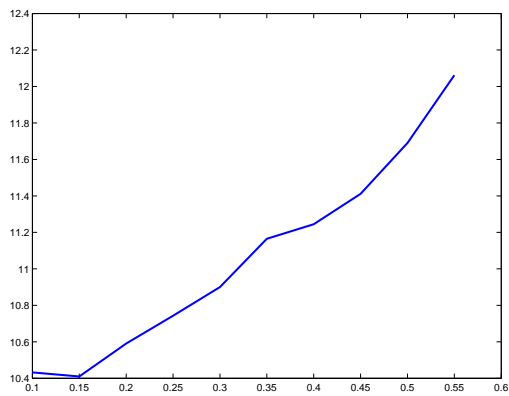
Fig. 9. CS deblurring for single-pixel cameras (SPMT). (a) original scene (left-upper part of Fig. 8). (b) single-step direct inverse. (c) our method with curvelet thresholding. (d) using  $H^{-1}$  instead of  $P^{-1}$  in our iterative method (i.e., using ICT but without PSI).



(a)



(b)



(c)

Fig. 10. Performances of SPMT as the number of measurements increases. (a) SNR (vertical coordinate) vs measurement numbers (horizontal coordinate). (b) Recovery error vs measurement numbers. (c) Computational time (unit: second) vs measurement numbers. The horizontal coordinate denotes the rate of practical measurements to total measurements.